Loci Periodic Surface Reconstruction from Crystals

Yan Wang

University of Central Florida, wangyan@mail.ucf.edu

ABSTRACT

Recently a periodic surface (PS) model for computer aided nano design (CAND) was proposed. This implicit surface model can parametrically create Euclidean and hyperbolic geometries at atomic, molecular, and mesoscopic scales while supporting symmetric tiling and crystal packing. In this paper, loci surface reconstruction from crystals is studied based on a generalized PS model.

Keywords: Periodic surface, implicit surface, computer-aided nano-design, reverse engineering.

1. INTRODUCTION

Computer-aided nano-design (CAND) is an extension of computer-based engineering design traditionally at bulk scales to nano scales. Enabling efficient structural descriptions is one of the key research issues in CAND. Traditional boundary-based parametric solid modeling methods do not support efficient construction of complex and dynamic nano-scale geometries due to some special characteristics at the low level. For instance, there are no clear-cut boundaries of atoms in a molecule. The Heisenberg uncertainty principle indicates the impossibility of simultaneously specifying the precise momentum and position of a particle at the quantum level. The volume packing of different atoms with clouds of correlated electrons is the central design theme at the atomic scale. Non-deterministic geometries and topologies are the manifestations of thermodynamic and kinetic properties at the molecular scale.

Traditional molecular visualization methods such as models of space-filled, wireframe, stick, ball-and-stick, ribbon and solvent-accessible surfaces do not support the parametric construction and modification of molecular structures. Parametric modeling mechanisms for particle aggregates at the molecular scale are needed to support rapid construction and optimization of geometries. At the meso scale, super-porous structures with high surface-volume ratios also need effective geometric descriptions. Providing nano engineers and scientists efficient and easy-to-use tools to create geometry conformation that is reasonably close to true minimum energy is highly desirable in material design.

With the observation that hyperbolic surfaces ubiquitously exist in nature and periodic features are common in condensed materials, we recently proposed an implicit surface modeling approach, periodic surface (herein referred to as PS), to represent geometric structures in nano scales [1, 2]. Periodic surfaces are either loci or foci. Loci surfaces are fictional continuous surfaces that pass through discrete particles in 3D space, whereas foci surfaces can be looked as isosurfaces of potential or density in which discrete particles are enclosed. The surface model allows for parametric construction from atomic scale to meso scale. In this paper, loci surface reconstruction for reverse engineering is studied. The PS model is generalized with both geometric and polynomial descriptions. An incremental searching algorithm is developed to reconstruct loci surfaces from crystals. In the remainder of the paper, Section 2 briefly reviews the related work in implicit surfaces and molecular surfaces. Section 3 generalizes the PS model to allow for the intuitive geometric interpretation of periodic basis vectors. Section 4 derives transformation properties of the PS model, which enable interactive manipulation of the implicit surfaces. Section 5 describes the incremental searching algorithm, presents several examples, and proposes two evaluation metrics for the quality of reconstructed surfaces.

2. BACKGROUND AND RELATED WORK

2.1 Implicit Surface

Implicit surfaces [3] are not as widely used as parametric surfaces in an interactive modeling environment, largely due to the lack of intuitive shape manipulation and control. Yet, implicit surface modeling has some advantages. For example, ray tracing is straightforward, and Boolean operations are closed. Research in implicit surface modeling includes the "blobby model" based on Gaussian function [4, 5], and polynomials [6]. Topics such as implicitization [7, 8], blending [9, 10], interpolation [11], control [12, 13], curvature formulation [14], as well as polygonization [15, 16] and direct ray tracing [17] have been studied.

2.2 Molecular Surface Modeling

For visualization purposes, there has been some research on surface modeling of molecular structures [18]. Lee and Richards [19] first introduced a solvent-accessible surface, the locus of a probe rolling over Van der Waals surface, to represent boundary of molecules. Connolly [20] presented an analytical method to calculate the surface. Recently, Carson [21] represented molecular surfaces with the B-spline wavelet. Edelsbrunner [22] described molecules with implicit-form skin surfaces. Bajaj et al. [23] represented solvent accessible surface by NURBS (non-uniform rational B-spline). Kim et al. [24] constructed NURBS molecular surfaces by the aid of Euclidean Voronoi diagrams. These research efforts concentrate on molecular visualization, whereas the construction support of molecular structures for design purposes is not considered.

2.3 Periodic Surface

We recently proposed a PS model to construct nano-scale geometries. It has the implicit form

$$\psi(\mathbf{r}) = \sum_k A_k \cos[2\pi(\mathbf{h}_k \cdot \mathbf{r})/\lambda_k + p_k] = C \tag{1}$$

where $\mathbf{r}$ is the location vector in Euclidean space $\mathbb{E}^3$, $\mathbf{h}_k$ is the k^{th} lattice vector in reciprocal space, A_k is the magnitude factor, λ_k is the wavelength of periods, p_k is the phase shift, and C is a constant. Specific periodic structures can be modeled based on this form. The periodic surface model can approximate triply periodic minimal surfaces (TPMSs) very well, which have been reported from atomic to meso scales. Compared to the parametric TPMS representation known as Weierstrass formula, PS models have a much simpler form and are easier to compute.

A periodic surface is specified by a periodic vector $(\mathbf{A},\mathbf{H},\mathbf{P},\mathbf{\Lambda})$ in a multi-dimensional configuration and phase space, where $\mathbf{A} = [A_k]$, $\mathbf{H} = [\mathbf{h}_k]$, $\mathbf{P} = [p_k]$, and $\mathbf{\Lambda} = [\lambda_k]$ are concatenations of magnitudes, reciprocal lattice vectors, phases, and period lengths, respectively. Increasing the dimension of the periodic vector, i.e., the number of control parameters, gives more degrees of freedom to model complex geometries. Fig. 1 lists some examples of PS models within one volumetric unit, including TPMS structures, such as P-, D-, G-, and I-WP cubic morphologies which are frequently referred to in chemistry literature. Besides the cubic phase, other mesophase structures such as spherical micelles, lamellar, rod alike hexagonal phases can also be modeled. The surfaces inherently satisfy periodic boundary conditions. Each surface divides the 3D space into two congruent labyrinth subspaces, which have the opposite + and – signs if the surface is $\psi(\mathbf{r}) = 0$.

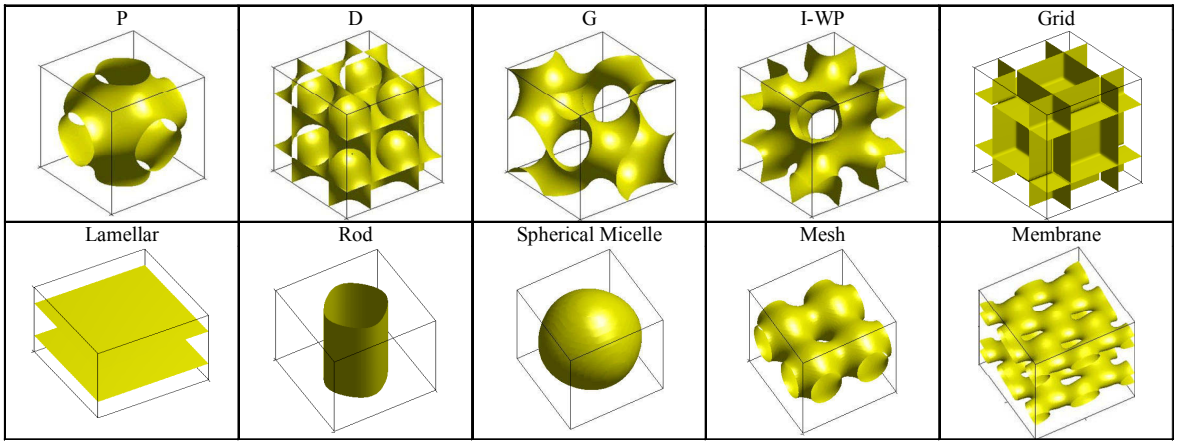

Fig. 1: Periodic surface models of cubic phase and mesophase structures [2].

3. GENERALIZED PERIODIC SURFACE MODEL

In this paper, the PS model is generalized with geometric and polynomial descriptions. A periodic surface is defined as

$$\psi(\mathbf{r}) = \sum_{l=1}^{L}\sum_{m=1}^{M} \mu_{lm} \cos\left(2\pi\kappa_l(\mathbf{p}_m^T \cdot \mathbf{r})\right) = 0 \tag{2}$$

where κ_l is the *scale parameter*, $\mathbf{p}_m = [a_m, b_m, c_m, \theta_m]^T$ is a *basis vector*, such as one of

$$\{\mathbf{e}_0,\mathbf{e}_1,\mathbf{e}_2,\mathbf{e}_3,\mathbf{e}_4,\mathbf{e}_5,\mathbf{e}_6,\mathbf{e}_7,\mathbf{e}_8,\mathbf{e}_9,\mathbf{e}_{10},\mathbf{e}_{11},\mathbf{e}_{12},\ldots\}=\left\{\begin{bmatrix}0\\0\\0\\1\end{bmatrix}\begin{bmatrix}1\\0\\0\\1\end{bmatrix}\begin{bmatrix}0\\1\\0\\1\end{bmatrix}\begin{bmatrix}0\\0\\1\\1\end{bmatrix}\begin{bmatrix}1\\1\\0\\1\end{bmatrix}\begin{bmatrix}1\\0\\1\\1\end{bmatrix}\begin{bmatrix}0\\1\\1\\1\end{bmatrix}\begin{bmatrix}1\\1\\1\\1\end{bmatrix}\begin{bmatrix}1\\-1\\0\\1\end{bmatrix}\begin{bmatrix}-1\\0\\1\\1\end{bmatrix}\begin{bmatrix}0\\1\\-1\\1\end{bmatrix}\begin{bmatrix}1\\-1\\1\\1\end{bmatrix}\begin{bmatrix}-1\\1\\1\\1\end{bmatrix}\ldots\right\} \quad (3)$$

which represents a *basis plane* in the projective 3-space $\mathbb{P}^3$, $\mathbf{r}=[x,y,z,w]^T$ is the location vector with homogeneous coordinates, and μ_{lm} is the *periodic moment*. Each basis vector represents a basis plane that is a 2D subspace in $\mathbb{P}^3$. Corresponding to a basis plane $\mathbf{p}_m$, $d_m=\hat{\mathbf{p}}_m^T\cdot\mathbf{r}=\mathbf{p}_m^T\cdot\mathbf{r}/\|\mathbf{p}_m\|$ is the projective distance between the origin and the projective subspace where $\mathbf{r}$ resides in. The projective distance is negative when the normal direction of the subspace is towards the origin, otherwise it is positive. We assume $w=1$ throughout this paper if w is not explicitly specified. It is also assumed that the scale parameters are natural integers ($\kappa_l\in\mathbb{N}$). The *degree* of $\psi(\mathbf{r})$ in Eqn. (2) is defined as $\deg(\psi(\mathbf{r})):=|\{\mathbf{p}_m\}|$, where $|A|$ is the cardinality of set *A*. The *scale* of $\psi(\mathbf{r})$ is defined as $\mathrm{sca}(\psi(\mathbf{r})):=|\{\kappa_l\}|$. This generalization allows for intuitive geometric interpretation of the periodic basis vectors and enables interactive manipulation such as affine transformations with homogeneous coordinates in $\mathbb{P}^3$.

If mapped to a *density space* $\mathbf{s}=[s_1,\ldots,s_M]^T$ where $s_m=\cos(2\pi(\mathbf{p}_m^T\cdot\mathbf{r}))$, $\psi(\mathbf{s})$ can be represented in a polynomial form, known as the Chebyshev polynomial,

$$\psi(\mathbf{s})=\sum_{l=1}^{L}\sum_{m=1}^{M}\mu_{lm}T_{\kappa_l}(s_m)\quad(|s_m|\le 1) \quad (4)$$

where $T_\kappa(s)=\cos(\kappa\cos^{-1}s)$. In a Hilbert space, a vector space with an inner product, the basis functions T_κ's are orthogonal to each other with respect to density in the normalized domain, with the inner product defined as

$$\langle T_i,T_j\rangle:=\int_{-1}^{1}\frac{1}{\sqrt{1-s^2}}T_i(s)T_j(s)ds=\begin{cases}0 & (i\ne j)\\ \pi & (i=j=0)\\ \pi/2 & (i=j\ne 0)\end{cases} \quad (5)$$

where both *i* and *j* are natural numbers ($i,j\in\mathbb{N}$). Orthonormal bases are particularly helpful in surface reconstruction. The periodic moments are determined by the projection

$$\mu_j=\frac{\langle f,T_j\rangle}{\langle T_j,T_j\rangle}=\frac{2}{\pi}\int_{-1}^{1}\frac{1}{\sqrt{1-s^2}}f(s)T_j(s)ds\quad(j\ne 0) \quad (6)$$

Two periodic surfaces $\psi_1(\mathbf{r})$ and $\psi_2(\mathbf{r})$ are called orthogonal if there exists a domain $\mathbb{D}=[\underline{x},\overline{x}]\times[\underline{y},\overline{y}]\times[\underline{z},\overline{z}]\times 1\subseteq\mathbb{R}^4$ such that $\langle\psi_1,\psi_2\rangle=\iiint_{\mathbb{D}}\psi_1(\mathbf{r})\psi_2(\mathbf{r})d\mathbf{r}=0$.

Lemma 1. If a surface $\psi(\mathbf{r})$ in Eq. (2) with the basis vectors $\{\mathbf{p}_m\}$ and the scale parameters $\{\kappa_l\}$ is scaled to $\psi'(\mathbf{r})$ with the new scale parameters $\{s\kappa_l\}$, and if there are no such basis vectors $\mathbf{p}_{m_1},\mathbf{p}_{m_2}\in\{\mathbf{p}_m\}(m_1\ne m_2)$ that satisfy $\kappa_i\mathbf{p}_{m_1}=s\kappa_j\mathbf{p}_{m_2}$ for some $\kappa_i,\kappa_j\in\{\kappa_l\}$, then $\psi(\mathbf{r})$ is orthogonal to $\psi'(\mathbf{r})$.

Proof. $\langle\psi,\psi'\rangle=\begin{cases}\frac{\pi}{2}\sum_{\kappa_i\mathbf{p}_{m1}=s\kappa_j\mathbf{p}_{m2}}\mu_{im_1}\mu_{jm_2} & \left(if\ \{\kappa_l\}\times\{\mathbf{p}_m\}\cap\{s\kappa_l\}\times\{\mathbf{p}_m\}\ne\varnothing\right)\\ 0 & \left(if\ \{\kappa_l\}\times\{\mathbf{p}_m\}\cap\{s\kappa_l\}\times\{\mathbf{p}_m\}=\varnothing\right)\end{cases}$. Thus, if there are no basis vectors $\mathbf{p}_{m_1},\mathbf{p}_{m_2}\in\{\mathbf{p}_m\}(m_1\ne m_2)$ that satisfy $\kappa_i\mathbf{p}_{m_1}=s\kappa_j\mathbf{p}_{m_2}$, then $\{\kappa_l\}\times\{\mathbf{p}_m\}\cap\{s\kappa_l\}\times\{\mathbf{p}_m\}=\varnothing$ □

Remark. If a periodic surface is scaled up or down, it is orthogonal to the original one if no common basis vectors at the same scales are found between the two.

4. TRANSFORMATION

As opposed to general implicit surfaces, transformations of periodic surfaces are more intuitive. Basis vectors play a central role here. Therefore, they provide users the handle for shape control and interactive manipulation of the implicit surfaces. In this section, the general affine transformation properties of periodic surfaces are derived as follows.

Lemma 2. Rotation of $\psi(\mathbf{r})$ about principle axes is equivalent to rotation of each of the basis vectors $\{\mathbf{p}_m\}$.

Proof. Let $\mathbf{R} = \begin{bmatrix} \cos\beta\cos\gamma & -\cos\beta\sin\gamma & \sin\beta & 0 \\ \cos\alpha\sin\gamma+\sin\alpha\sin\beta\cos\gamma & \cos\alpha\cos\gamma-\sin\alpha\sin\beta\sin\gamma & -\sin\alpha\cos\beta & 0 \\ \sin\alpha\sin\gamma-\cos\alpha\sin\beta\cos\gamma & \sin\alpha\cos\gamma+\cos\alpha\sin\beta\sin\gamma & \cos\alpha\cos\beta & 0 \\ 0 & 0 & 0 & 1 \end{bmatrix}$ where α, β, and γ are the rotation angles about *x*, *y*, and *z* axes respectively.

$$\psi(\mathbf{R}^{-1}\cdot\mathbf{r}) = \sum_{l=1}^{L}\sum_{m=1}^{M}\mu_{lm}\cos\left(2\pi\kappa_l(\mathbf{p}_m^T\cdot(\mathbf{R}^{-1}\cdot\mathbf{r}))\right) = \sum_{l=1}^{L}\sum_{m=1}^{M}\mu_{lm}\cos\left(2\pi\kappa_l(\mathbf{p}_m^T\cdot\mathbf{R}^T\cdot\mathbf{r})\right)$$

$$= \sum_{l=1}^{L}\sum_{m=1}^{M}\mu_{lm}\cos\left(2\pi\kappa_l((\mathbf{R}\cdot\mathbf{p}_m)^T\cdot\mathbf{r})\right) \qquad \square$$

Lemma 3. Translation is equivalent to offsetting each of the basis planes corresponding to the basis vectors $\{\mathbf{p}_m\}$.

Proof. Let $\mathbf{T} = \begin{bmatrix} 1 & 0 & 0 & t_x \\ 0 & 1 & 0 & t_y \\ 0 & 0 & 1 & t_z \\ 0 & 0 & 0 & 1 \end{bmatrix}$, $\mathbf{T}_t = \left(\mathbf{T}^{-1}\right)^T = \begin{bmatrix} 1 & 0 & 0 & 0 \\ 0 & 1 & 0 & 0 \\ 0 & 0 & 1 & 0 \\ -t_x & -t_y & -t_z & 1 \end{bmatrix}$.

$$\psi(\mathbf{T}^{-1}\cdot\mathbf{r}) = \sum_{l=1}^{L}\sum_{m=1}^{M}\mu_{lm}\cos\left(2\pi\kappa_l(\mathbf{p}_m^T\cdot\mathbf{T}_t^T\cdot\mathbf{r})\right) = \sum_{l=1}^{L}\sum_{m=1}^{M}\mu_{lm}\cos\left(2\pi\kappa_l((\mathbf{T}_t\cdot\mathbf{p}_m)^T\cdot\mathbf{r})\right)$$

$$\mathbf{T}_t\cdot\mathbf{p}_m = [a_m, b_m, c_m, \theta_m - (a_m t_x + b_m t_y + c_m t_z)]^T \qquad \square$$

Lemma 4. Scaling and reflection are equivalent to their respective inverse operations on each of the basis vectors $\{\mathbf{p}_m\}$.

Proof. Let $\mathbf{S} = \begin{bmatrix} s_x & 0 & 0 & 0 \\ 0 & s_y & 0 & 0 \\ 0 & 0 & s_z & 0 \\ 0 & 0 & 0 & 1 \end{bmatrix}$, $\mathbf{S}_s = \mathbf{S}^{-1} = \begin{bmatrix} 1/s_x & 0 & 0 & 0 \\ 0 & 1/s_y & 0 & 0 \\ 0 & 0 & 1/s_z & 0 \\ 0 & 0 & 0 & 1 \end{bmatrix}$.

$$\psi(\mathbf{S}^{-1}\cdot\mathbf{r}) = \sum_{l=1}^{L}\sum_{m=1}^{M}\mu_{lm}\cos\left(2\pi\kappa_l(\mathbf{p}_m^T\cdot\mathbf{S}_s{}^T\cdot\mathbf{r})\right) = \sum_{l=1}^{L}\sum_{m=1}^{M}\mu_{lm}\cos\left(2\pi\kappa_l((\mathbf{S}_s\cdot\mathbf{p}_m)^T\cdot\mathbf{r})\right) \qquad \square$$

5. LOCI SURFACE RECONSTRUCTION

3D crystal or protein structures are usually inferred by using experimental techniques such as X-ray crystallography then archived in structure databases. Given the actual crystal structures, periodic loci surface models can be reconstructed. This reverse engineering process is helpful in nano material design. It can be widely applied in material re-engineering and re-design, comparison and analysis of unknown structures, and improving interoperability of different models. In general, the loci surface reconstruction process is to find a $\psi(\mathbf{r})$ to approximate the original but unknown surface $f(\mathbf{r})$, assuming that there always exists a fictional continuous surface $f(\mathbf{r})$ that passes through a finite number of discrete locations in $\mathbb{E}^3$. Determining periodic moments from the given locations is the goal.

5.1 Incremental Searching Algorithm

In the case of sparse location data, spectral analysis is helpful in deriving periodic moments. Given *N* known positions

$\mathbf{r}_n \in \mathbb{P}^3$ $(n = 1,\ldots,N)$ through which a loci surface passes, loci surface reconstruction is to find a $\psi(\mathbf{r}) = 0$ such that the sum of Lp norms is minimized in

$$\min \sum_{n=1}^{N} \left\| \psi(\mathbf{r}_n) \right\|_p \tag{7}$$

Given a set of scale parameters κ_l $(l = 1,\ldots,L)$ and a set of basis vectors $\mathbf{p}_m$ $(m = 1,\ldots,M)$, deriving the moments can be reduced to solving the linear system

$$\sum_{l=1}^{L} \sum_{m=1}^{M} \cos\left(2\pi\kappa_l(\mathbf{p}_m^T \cdot \mathbf{r}_n)\right)\mu_{lm} = 0 \quad (n = 1,\ldots,N) \tag{8}$$

or simply denoted as

$$\mathbf{A}_{N\times LM}\boldsymbol{\mu}_{LM\times 1} = 0 \tag{9}$$

Solving Eqn.(9) is to find the null space of $\mathbf{A}$. The singular value decomposition (SVD) method can be applied. If the decomposed matrix is $\mathbf{A} = [u_i]_{N\times LM}[w_j]_{LM\times LM}[v_k]^T_{LM\times LM}$, any column of $[v_k]$ whose corresponding w_j is zero yields a solution. With the consideration of experimental or numerical errors, least-square approximation is usually used in actual algorithm implementations. For instance, we can select the last column of $[v_k]$ as the approximated solution.

In general cases, the periodic vectors and scale parameters may be unknown, an incremental searching algorithm is developed to search moments as well as periodic vectors and scale parameters, as shown in Fig. 2. We can use a general set of periodic vectors such as the one in Eqn. (3) and incrementally reduce scales, i.e., increase the scale parameters. The searching process continues until the *maximum approximation error* $\max_n \left|\psi(\mathbf{r}_n)\right|$ is less than a pre-determined threshold.

Input: location vectors $\mathbf{r}_n$ $(n = 1,\ldots,N)$

Output: periodic moments $\{\mu_{lm}\}$, scale parameters $\{\kappa_l\}$, and periodic vectors $\{\mathbf{p}_m\}$

1. Normalize coordinates $\mathbf{r}_n$ if necessary (e.g. limit them within the range of [0,1]);
2. Set an error threshold ε;
3. Initialize periodic vectors $\{\mathbf{p}_m\}^{(0)} = \{\mathbf{e}_0\}$, initialize scale parameter $\{\kappa_l\}^{(0)} = \{1\}$, t=1;
4. Update the periodic vectors $\{\mathbf{p}_m\}^{(t)} = \{\mathbf{p}_m\}^{(t-1)} \cup \{\mathbf{e}_1,\ldots,\mathbf{e}_M\}$, update the scale parameters with a new scale s_t so that $\{\kappa_l\}^{(t)} = \{\kappa_l\}^{(t-1)} \cup \{s_t\}$;
5. Decompose matrix $\mathbf{A}^{(t)} = \left[\cos\left(2\pi\kappa_l(\mathbf{p}_m^T \cdot \mathbf{r}_n)\right)\right] = \mathbf{UWV}^T$ and find $\boldsymbol{\mu}^{(t)}$ as the last column of $\mathbf{V}$;
6. If $\max_n \left|\mathbf{A}^{(t)} \cdot \boldsymbol{\mu}^{(t)}\right| < \varepsilon$, stop; otherwise, t=t+1, go to Step 4 and repeat.

Fig. 2: Incremental searching algorithm for loci surface reconstruction.

In the Hilbert space, the orthogonality of periodic basis functions enables a concise representation in reconstruction. In the incremental searching, the newly created small scale information in iteration t is an approximation of the difference between the original surface $f(\mathbf{r})$ and the previously constructed surface $\psi^{(t-1)}(\mathbf{r})$ in iteration $t-1$.

Lemma 5. If the original surface $f(\mathbf{r})$ is d times continuously differentiable, the convergence rate of the incremental searching algorithm is $O(\kappa^{-d})$ where κ is the scale parameter.

Proof. According to Eqn. (6), for any target surface $f(s)$, a periodic moment at the scale κ is

$$\mu_\kappa = \frac{2}{\pi}\int_{-1}^{1} \frac{1}{\sqrt{1-s^2}} f(s)\cos\left(\kappa\cos^{-1}(s)\right)ds \tag{10}$$

Because of

$$\frac{d\sin\left(\kappa\cos^{-1}(s)\right)}{ds} = -\frac{\kappa}{\sqrt{1-s^2}}\cos\left(\kappa\cos^{-1}(s)\right) \text{ and } \frac{d\cos\left(\kappa\cos^{-1}(s)\right)}{ds} = \frac{\kappa}{\sqrt{1-s^2}}\sin\left(\kappa\cos^{-1}(s)\right),$$

continuously applying the rule of partial integration to Eqn. (10), we have

$$\begin{aligned}
\mu_\kappa &= \frac{1}{\kappa}\cdot\frac{2}{\pi}\int_{-1}^{1}\sin\left(\kappa\cos^{-1}(s)\right)f'(s)ds \\
&= \frac{1}{\kappa^2}\cdot\frac{2}{\pi}\int_{-1}^{1}\frac{1}{\sqrt{1-s^2}}\cos\left(\kappa\cos^{-1}(s)\right)\left[sf'(s)-(1-s^2)f''(s)\right]ds \\
&= \frac{1}{\kappa^3}\cdot\frac{2}{\pi}\int_{-1}^{1}\sin\left(\kappa\cos^{-1}(s)\right)\left[f'(s)+3sf''(s)-(1-s^2)f'''(s)\right]ds \\
&= \frac{1}{\kappa^4}\cdot\frac{2}{\pi}\int_{-1}^{1}\frac{1}{\sqrt{1-s^2}}\cos\left(\kappa\cos^{-1}(s)\right)\left[sf'(s)-(4-7s^2)f''(s)-(6s+6s^3)f'''(s)+(1-s^2)^2f^{(4)}(s)\right]ds \\
&= \dots \\
&= \begin{cases}
\frac{1}{\kappa^d}\cdot\frac{2}{\pi}\int_{-1}^{1}\sin\left(\kappa\cos^{-1}(s)\right)\left[\sum_{j=1}^{d}h(s)f^{(j)}(s)\right]ds & when\ d\ is\ odd \\
\frac{1}{\kappa^d}\cdot\frac{2}{\pi}\int_{-1}^{1}\frac{1}{\sqrt{1-s^2}}\cos\left(\kappa\cos^{-1}(s)\right)\left[\sum_{j=1}^{d}h(s)f^{(j)}(s)\right]ds & when\ d\ is\ even
\end{cases}
\end{aligned}$$

Since $-1 \le s \le 1$, $\left|\cos\left(\kappa\cos^{-1}(s)\right)\right| \le 1$, $\left|\sin\left(\kappa\cos^{-1}(s)\right)\right| \le 1$, and $\left|\sum_{j=1}^{d}h(s)f^{(j)}(s)\right| \le \infty$, there exists a constant C such that

$$\mu_\kappa \le \frac{1}{\kappa^d}\cdot\frac{2}{\pi}C$$

□

5.2 Examples

For the first example, we reconstruct the periodic surface model of a Faujasite crystal, a type of zeolite minerals which can be widely used as molecular sieves and catalysts in pollution control, detergent, manufacturing, etc. As shown in Fig. 3-a, each vertex in the polygon model represents a Si atom of the crystal. Within a periodic unit, we apply the incremental searching algorithm and reconstruct two surfaces with 14 and 15 vectors for different stopping criteria, as shown in Fig. 3-b and Fig. 3-c respectively. The reconstructed PS models are listed in Tab. 1.

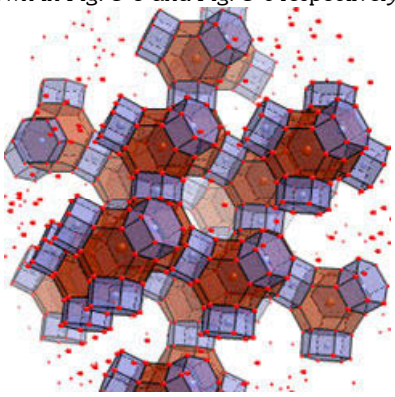

(a) Faujasite crystal. Each tetradecahedron encloses a **Fe**, each hexagonal prism encloses an **Al**, and each vertex of the polygons represents a **Si**.

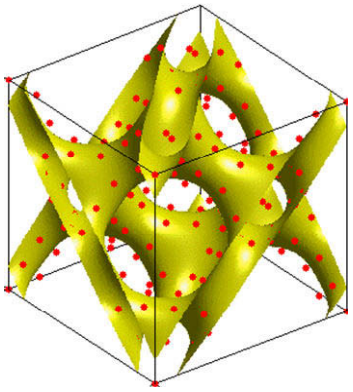

(b) Reconstructed surface dim.=14, max_error=0.6691

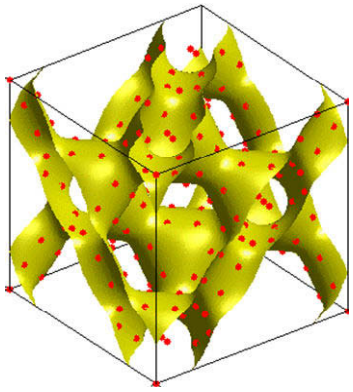

(c) Reconstructed surface dim.=15, max_error= 1.686e-15

Fig. 3: Loci surfaces of a Faujasite crystal with 232 atoms.

The second example is a PS model of a synthetic Zeolite crystal. As shown in Fig. 4-a. Each vertex of the polygon model represents an O atom. Three surfaces with different numbers of vectors thus different resolutions are shown in Fig. 4-b, -c, and -d. The reconstructed PS models are listed in Tab. 2.

Dimension	PS model
14	$-0.53909 - 0.0085926\cos(2\pi x) - 0.0085926\cos(2\pi y) - 0.0085926\cos(2\pi z) - 0.0039482\cos(2\pi(x+y)) - 0.0039482\cos(2\pi(x+z))$ $- 0.0039482\cos(2\pi(y+z)) - 0.011992\cos(2\pi(x-y)) - 0.011992\cos(2\pi(z-x)) - 0.011992\cos(2\pi(y-z))$ $- 0.44082\cos(2\pi(x+y+z)) + 0.41407\cos(2\pi(x-y+z)) + 0.41407\cos(2\pi(y+z-x)) + 0.41407\cos(2\pi(x+y-z))$
15	$0.51662 + 0.40246\cos(2\pi(x+y+z)) - 0.40246\cos(2\pi(x-y+z)) - 0.40246\cos(2\pi(y+z-x))$ $- 0.40246\cos(2\pi(x+y-z)) - 0.10362\cos(4\pi(x+y)) - 0.10362\cos(4\pi(x+z))$ $- 0.10362\cos(4\pi(y+z)) + 0.10362\cos(4\pi(x-y)) + 0.10362\cos(4\pi(z-x)) + 0.10362\cos(4\pi(y-z))$ $+ 0.072076\cos(4\pi(x+y+z)) + 0.072076\cos(4\pi(x-y+z)) + 0.072076\cos(4\pi(y+z-x)) + 0.072076\cos(4\pi(x+y-z))$

Tab. 1: PS models of the Faujasite crystal in Fig. 3 with different dimensions.

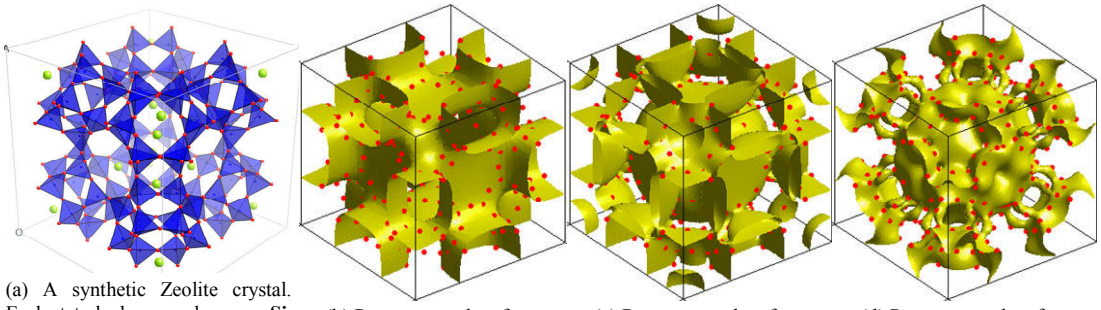

(a) A synthetic Zeolite crystal. Each tetrahedron encloses a **Si**, each vertex of the tetrahedral is a **O**, and each green sphere is a **Na**.

(b) Reconstructed surface dim.=14, max_error=0.2515

(c) Reconstructed surface dim.=24, max_error=0.0092

(d) Reconstructed surface dim.=33, max_error=3.059e-15

Fig. 4: Loci surfaces of a synthetic Zeolite crystal with 312 atoms.

Dimension	PS model
14	$-0.0037436 - 0.28887\cos(2\pi x) - 0.28887\cos(2\pi y) - 0.28887\cos(2\pi z) + 0.001388\cos(2\pi(x+y)) + 0.001388\cos(2\pi(x+z))$ $+ 0.001388\cos(2\pi(y+z)) + 0.001388\cos(2\pi(x-y)) + 0.001388\cos(2\pi(z-x)) + 0.001388\cos(2\pi(y-z))$ $- 0.43291\cos(2\pi(x+y+z)) - 0.43291\cos(2\pi(x-y+z)) - 0.43291\cos(2\pi(y+z-x)) - 0.43291\cos(2\pi(x+y-z))$
24	$-0.16232 + 0.18191\cos(2\pi(x+y)) + 0.18191\cos(2\pi(x+z))$ $+ 0.18191\cos(2\pi(y+z)) + 0.18191\cos(2\pi(x-y)) + 0.18191\cos(2\pi(z-x)) + 0.18191\cos(2\pi(y-z))$ $+ 0.00071864\cos(2\pi(x+y+z)) + 0.00071864\cos(2\pi(x-y+z)) + 0.00071864\cos(2\pi(y+z-x)) + 0.00071864\cos(2\pi(x+y-z))$ $- 0.32147\cos(4\pi x) - 0.32147\cos(4\pi y) - 0.32147\cos(4\pi z) - 0.24617\cos(4\pi(x+y)) - 0.24617\cos(4\pi(x+z))$ $- 0.24617\cos(4\pi(y+z)) - 0.24617\cos(4\pi(x-y)) - 0.24617\cos(4\pi(z-x)) - 0.24617\cos(4\pi(y-z))$ $- 0.15927\cos(4\pi(x+y+z)) - 0.15927\cos(4\pi(x-y+z)) - 0.15927\cos(4\pi(y+z-x)) - 0.15927\cos(4\pi(x+y-z))$
33	$0.01531 + 0.37384\cos(2\pi(x+y)) + 0.37384\cos(2\pi(x+z))$ $+ 0.37384\cos(2\pi(y+z)) + 0.37384\cos(2\pi(x-y)) + 0.37384\cos(2\pi(z-x)) + 0.37384\cos(2\pi(y-z))$ $- 0.086043\cos(4\pi x) - 0.086043\cos(4\pi y) - 0.086043\cos(4\pi z) - 0.098288\cos(4\pi(x+y)) - 0.098288\cos(4\pi(x+z))$ $- 0.098288\cos(4\pi(y+z)) - 0.098288\cos(4\pi(x-y)) - 0.098288\cos(4\pi(z-x)) - 0.098288\cos(4\pi(y-z))$ $- 0.020038\cos(4\pi(x+y+z)) - 0.020038\cos(4\pi(x-y+z)) - 0.020038\cos(4\pi(y+z-x)) - 0.020038\cos(4\pi(x+y-z))$ $- 0.11405\cos(8\pi x) - 0.11405\cos(8\pi y) - 0.11405\cos(8\pi z) - 0.081757\cos(8\pi(x+y)) - 0.081757\cos(8\pi(x+z))$ $- 0.081757\cos(8\pi(y+z)) - 0.081757\cos(8\pi(x-y)) - 0.081757\cos(8\pi(z-x)) - 0.081757\cos(8\pi(y-z))$ $+ 0.0091814\cos(8\pi(x+y+z)) + 0.0091814\cos(8\pi(x-y+z)) + 0.0091814\cos(8\pi(y+z-x)) + 0.0091814\cos(8\pi(x+y-z))$

Tab. 2: PS models of the synthetic Zeolite crystal in Fig. 4 with different dimensions.

5.3 Quality of Reconstructed Surface

The maximum approximation error used in the incremental searching algorithm should not be the only metric to measure the quality of reconstructed surfaces. It should be noted that the maximum approximation error may cause overfitting during the least square error reconstruction due to the following lemma.

Lemma 6. Given any finite number of positions $\mathbf{r}_n \in \mathbb{P}^3$ $(n = 1,\ldots,N)$, there is always a $\psi(\mathbf{r}) = 0$ with finite degrees and scales such that $\psi(\mathbf{r}_n) = 0$ $(n = 1,\ldots,N)$.

Proof. If $n = 1$, we can construct a surface $\psi(\mathbf{r}) = \cos\left(\frac{x}{3x_0} + \frac{y}{3y_0} + \frac{z}{3z_0}\right) = 0$ for the known position $\mathbf{r}_1 = (x_0, y_0, z_0, 1)$.

Suppose there are two surfaces $\psi_a(\mathbf{r}) = 0$ and $\psi_b(\mathbf{r}) = 0$ that are constructed by two sets of positions $\{\mathbf{r}_i^a\}(i = 1,\ldots,N_a)$ and $\{\mathbf{r}_j^b\}(j = 1,\ldots,N_b)$ respectively. Since $\cos\alpha\cos\beta = \frac{1}{2}\cos(\alpha+\beta) + \frac{1}{2}\cos(\alpha-\beta)$ for any $\alpha, \beta \in \mathbb{R}$, we can always construct a third surface $\psi(\mathbf{r}) = \psi_a(\mathbf{r}) \cdot \psi_b(\mathbf{r}) = 0$ such that $\psi(\mathbf{r}_n) = 0$ for $\forall \mathbf{r}_n \in \{\mathbf{r}_i^a\} \cup \{\mathbf{r}_j^b\}$. □

To avoid overfitting potentially caused by the maximum approximation error, we use *porosity* as another metric to measure the quality of reconstructed loci surfaces, which is defined as

$$\phi := \iiint_{\mathbf{r}\in\mathbb{D}} \left(\psi(\mathbf{r})/\psi_M\right)^2 d\mathbf{r} \Big/ \iiint_{\mathbf{r}\in\mathbb{D}} d\mathbf{r} \quad (\mathbb{D} \subseteq \mathbb{P}^3) \tag{11}$$

where $\psi_M = \max_{\forall \mathbf{r}\in\mathbb{D}} |\psi(\mathbf{r})|$. ϕ measures the average absolute value of the implicit function evaluation within a volumetric unit. Notice that $\psi(\mathbf{r}) = 0$ at any location $\mathbf{r}$ where the surface passes through. Thus the higher the surface-volume ratio is, the lower the porosity will be. The porosities of the reconstructed surfaces in Fig. 3 and Fig. 4 are listed in Tab. 3. Given a fixed number of known positions that surfaces pass through, there are an infinite number of surfaces that can be reconstructed. Intuitively, the surfaces with unnecessarily high surface areas have low porosities, which should be avoided.

	Dimension	Maximum approximation error	Porosity
Faujasite surface (Fig. 3)	14	0.6691	0.2115
	15	1.686e-15	0.1226
Zeolite surface (Fig. 4)	14	0.2515	0.00738
	24	0.0092	0.0394
	33	3.059e-15	0.0829

Tab. 3: Metrics comparison of different PS surfaces.

The quality of reconstructed surfaces depends on the selection of periodic vectors, scale parameters, and volumetric domain of periodic units. Based on the porosity metric, we can optimize the surface reconstruction by solving

$$\begin{aligned} &\max \phi\left(\{\mathbf{p}_m\}, \{\kappa_l\}, \mathbb{D}\right) \\ &s.t. \max_n |\psi(\mathbf{r}_n)| \le \varepsilon \quad (n = 1,\ldots,N) \end{aligned} \tag{12}$$

where porosity is a function of $\{\mathbf{p}_m\}$, $\{\kappa_l\}$, and $\mathbb{D}$. Any of these parameters can be optimized. We apply Eqn. (12) to optimize the basis vectors of the PS model of the Zeolite crystal in Fig. 4-d. The result is shown in Fig. 5 and Tab. 4. The dimension is reduced from 33 to 25 while the porosity is increased to 0.1140 with a similar maximum approximation error.

	Optimized PS model
Dimension =25 Porosity =0.1140 Max Approx. Error =2.1417e-15	$-0.038986 - 0.37489\cos(2\pi(x+y)) - 0.37489\cos(2\pi(x+z))$ $- 0.37489\cos(2\pi(y+z)) - 0.37489\cos(2\pi(x-y)) - 0.37489\cos(2\pi(z-x)) - 0.37489\cos(2\pi(y-z))$ $+ 0.036561\cos(4\pi x) + 0.036561\cos(4\pi y) + 0.036561\cos(4\pi z) + 0.072615\cos(4\pi(x+y)) + 0.072615\cos(4\pi(x+z))$ $+ 0.072615\cos(4\pi(y+z)) + 0.072615\cos(4\pi(x-y)) + 0.072615\cos(4\pi(z-x)) + 0.072615\cos(4\pi(y-z))$ $+ 0.13904\cos(8\pi x) + 0.13904\cos(8\pi y) + 0.13904\cos(8\pi z) + 0.1013\cos(8\pi(x+y)) + 0.1013\cos(8\pi(x+z))$ $+ 0.1013\cos(8\pi(y+z)) + 0.1013\cos(8\pi(x-y)) + 0.1013\cos(8\pi(z-x)) + 0.1013\cos(8\pi(y-z))$

Tab. 4: Optimized PS model of the Zeolite crystal in Fig. 4-d.

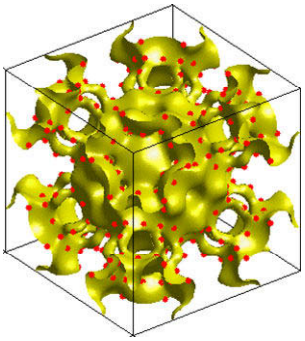

Fig. 5: Optimized Zeolite surface in Fig. 4-d.

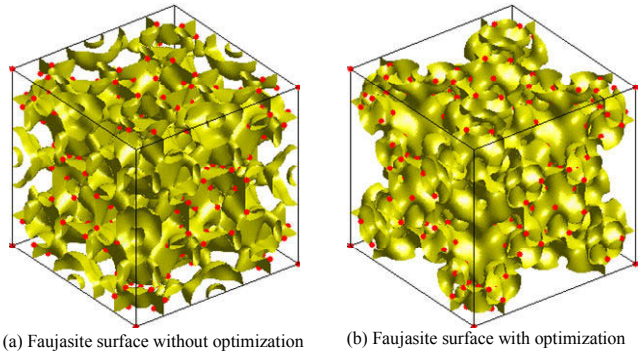

(a) Faujasite surface without optimization (b) Faujasite surface with optimization

Fig. 6: Surface comparison of the Faujasite crystal within a new periodic unit.

As a second example, the optimization process is applied to the PS models of the Faujasite crystal in Fig. 3 to find an optimal phase shift θ in all periodic vectors. It turns out that the phase shift of zeros in Fig. 3-c is optimal. We change the volumetric domain of the periodic unit. A different surface is reconstructed, as reconstruction is domain dependent. The results from the incremental searching algorithm are compared both with and without optimization in Fig. 6 and Tab. 5. During the optimization, some portions of the surface which do not pass through any atoms are removed. This illustrates the direct effect of considering porosity during reconstruction.

	PS model
Without optimization Porosity =0.0635 Max Approx. Error	$-0.023878 - 0.11551\cos(2\pi(x+y+z)) - 0.11551\cos(2\pi(x-y+z)) - 0.11551\cos(2\pi(y+z-x)) - 0.11551\cos(2\pi(x+y-z))$ $+ 0.090823\cos(4\pi x) + 0.090823\cos(4\pi y) + 0.090823\cos(4\pi z) - 0.30295\cos(4\pi(x+y)) - 0.30781\cos(4\pi(x+z)) - 0.30026\cos(4\pi(y+z))$ $- 0.30295\cos(4\pi(x-y)) - 0.30781\cos(4\pi(z-x)) - 0.30026\cos(4\pi(y-z)) - 0.010361\cos(4\pi(x+y+z)) - 0.010361\cos(4\pi(x-y+z))$ $- 0.010361\cos(4\pi(y+z-x)) - 0.010361\cos(4\pi(x+y-z)) + 0.10473\cos(8\pi x) + 0.11596\cos(8\pi y) + 0.10873\cos(8\pi z) + 0.22419\cos(8\pi(x+y))$ $+ 0.22254\cos(8\pi(x+z)) + 0.26375\cos(8\pi(y+z)) + 0.15627\cos(8\pi(x-y)) + 0.13716\cos(8\pi(z-x)) + 0.12819\cos(8\pi(y-z))$ $+ 0.081645\cos(8\pi(x+y+z)) + 0.18339\cos(8\pi(x-y+z)) + 0.15829\cos(8\pi(y+z-x)) + 0.19211\cos(8\pi(x+y-z))$

=1.9706e-15	
With optimization Porosity =0.0715 Max Approx. Error =5.038e-5	$-0.26028 + 0.34162\cos(2\pi(x+y+z+\theta^*)) + 0.34162\cos(2\pi(x-y+z+\theta^*)) + 0.34162\cos(2\pi(y+z-x+\theta^*))$ $+ 0.34162\cos(2\pi(x+y-z+\theta^*)) - 0.26862\cos(4\pi(x+\theta^*)) - 0.26862\cos(4\pi(y+\theta^*))$ $- 0.26862\cos(4\pi(z+\theta^*)) + 0.01134\cos(4\pi(x+y+\theta^*)) + 0.010794\cos(4\pi(x+z+\theta^*))$ $+ 0.012355\cos(4\pi(y+z+\theta^*)) + 0.011341\cos(4\pi(x-y+\theta^*)) + 0.010796\cos(4\pi(z-x+\theta^*)) + 0.012356\cos(4\pi(y-z+\theta^*))$ $+ 0.03066\cos(4\pi(x+y+z+\theta^*)) + 0.030639\cos(4\pi(x-y+z+\theta^*)) + 0.030639\cos(4\pi(y+z-x+\theta^*))$ $+ 0.030639\cos(4\pi(x+y-z+\theta^*)) + 0.15014\cos(8\pi(x+\theta^*)) + 0.15247\cos(8\pi(y+\theta^*))$ $+ 0.15165\cos(8\pi(z+\theta^*)) - 0.14607\cos(8\pi(x+y+\theta^*)) - 0.14644\cos(8\pi(x+z+\theta^*))$ $- 0.14624\cos(8\pi(y+z+\theta^*)) + 0.026281\cos(8\pi(x-y+\theta^*)) + 0.024318\cos(8\pi(z-x+\theta^*)) + 0.030786\cos(8\pi(y-z+\theta^*))$ $- 0.01715\cos(8\pi(x+y+z+\theta^*)) - 0.19186\cos(8\pi(x-y+z+\theta^*)) - 0.18873\cos(8\pi(y+z-x+\theta^*)) - 0.19107\cos(8\pi(x+y-z+\theta^*))$ where $\theta^* = 0.00011295$

Tab. 5: PS models without and with optimization of phase shift.

6. CONCLUDING REMARKS

In this paper, loci surface reconstruction is studied based on a generalized periodic surface model. Transformation properties of the implicit surface model are derived to support user interactive manipulation. An incremental searching algorithm is developed to reconstruct loci surfaces from crystals. The maximum approximation error and porosity are proposed to measure the quality of the reconstructed surface. An optimization method for surface reconstruction based on the metrics is developed. Future research will include the reconstruction of foci surfaces.

7. ACKNOWLEGEMENTS

This work is supported in part by the NSF CAREER Award CMMI-0645070. The author appreciates the reviewers' comments for improvement of the paper.

8. REFERENCES

[1] Wang, Y.: Geometric modeling of nano structures with periodic surfaces, Lecture Notes in Computer Science, 4077, 2006, 343-356
[2] Wang, Y.: Periodic surface modeling for computer aided nano design, Computer-Aided Design, 39(3), 2007, 179-189.
[3] Bloomenthal, J.: Introduction to Implicit Surfaces, Morgan Kaufmann, San Francisco, CA, 1997
[4] Blinn, J. F.: A generalization of algebraic surface drawing, ACM Transactions on Graphics, 1(3), 1982, 235-256
[5] Muraki, S.: Volumetric shape description of range data using "blobby model", Computer Graphics, 25(4), 1991, 227-235.
[6] Sederberg, T. W.: Surfaces: Techniques for cubic algebraic surfaces, IEEE Computer Graphics & Applications, 10(4), 1991, 14-25
[7] Sederberg, T. W.; Anderson, D. C.; Goldman, R.N.: Implicit representation of parametric curves and surfaces, Computer Vision, Graphics, & Image Processing, 28(1), 1984, 72-84
[8] Hoffmann, C. M.: Implicit curves and surfaces in CAGD, IEEE Computer Graphics & Applications, 16(3), 1993, 245-254
[9] Warren, J.: Blending algebraic surfaces, ACM Transactions on Graphics, 8(4), 1989, 263-278
[10] Hartmann, E.: Blending an implicit with a parametric surface, Computer Aided Geometric Design, 12(8), 1995, 825-835
[11] Turk, G.; O'brien, J. F.: Modeling with implicit surfaces that interpolate, ACM Transactions on Graphics, 21(4), 2002, 855-873
[12] Sederberg, T.: Piecewise algebraic surface patches, Computer Aided Geometric Design, 2(1-3), 1985, 53-60
[13] Witkin, A. P.; Heckbert, P. S.: Using particles to sample and control implicit surfaces, Proc. 1994 SIGGRAPH, 269-277
[14] Goldman, R.: Curvature formulas for implicit curves and surfaces, Computer Aided Geometric Design, 22(7), 2005, 623-658

[15] Wyvill, G.; McPheeters, C.; Wyvill, B.: Data structure for soft objects, The Visual Computer, 2(2), 1986, 227-234
[16] Bloomenthal, J.: Polygonization of implicit surfaces, Computer Aided Geometric Design, 5(4), 1988, 341-355
[17] Hart, J.: Sphere tracing: a geometric method for the antialiased ray tracing of implicit surfaces, The Visual Computer, 12(10), 1996, 527-545
[18] Connolly, M. L.: Molecular surfaces: A review, Network Science, 1996, http://www.netsci.org/Science/Compchem/index.html
[19] Lee, B.; Richards, F.M.: The interpretation of protein structures: Estimation of static accessibility, Journal of Molecular Biology, 55(3), 1971, 379-400
[20] Connolly, M. L.: Solve-accessible surfaces of proteins and nucleic acids, Science, 221(4612), 1983, 709-713
[21] Carson, M: Wavelets and molecular structure, J. of Computer Aided Molecular Design, 10(4), 1996, 273-283
[22] Edelsbrunner, H.: Deformable smooth surface design, Discrete & Computational Geometry, 21(1), 1999, 87-115
[23] Bajaj, C.; Pascucci, V.; Shamir, A.; Holt, R.; Netravali, A.: Dynamic Maintenance and visualization of molecular surfaces, Discrete Applied Mathematics, 127(1), 2003, 23-51
[24] Ryu, J.; Kim, D.; Cho, Y.; Park, R. and Kim, D.-S.: Computation of molecular surface using Euclidean Voronoi Diagram, Computer-Aided Design & Applications, 2(1-4), 2005, 439-448